

Effect of Copper Donor Material Assisted Friction Stir Welding of AA6061-T6 Alloy On Downward Force, Microstructure, And Mechanical Properties

Srinivasa Bhukya

Virginia State University

Zhenhua Wu (✉ zhu@vsu.edu)

Virginia State University

Joseph Maniscalco

Old Dominion University

Abdelmageed Elmustafa

Old Dominion University

Research Article

Keywords: Al6061-T6 alloy, Cu Donor material, Friction stir welding, Microstructure, Micro-hardness, Tensile properties, Fractography

Posted Date: August 20th, 2021

DOI: <https://doi.org/10.21203/rs.3.rs-817019/v1>

License:  This work is licensed under a Creative Commons Attribution 4.0 International License. [Read Full License](#)

Version of Record: A version of this preprint was published at The International Journal of Advanced Manufacturing Technology on January 4th, 2022. See the published version at <https://doi.org/10.1007/s00170-021-08390-8>.

Abstract

In this research, Copper (Cu) donor material assisted friction stir welding (FSW) of AA6061-T6 alloy was studied. Cu assisted FSW joints of AA6061-T6 alloy were prepared at a constant tool rotational rate of 1400 rpm and various welding speeds at 1 mm/s and 3 mm/s. The Cu donor material of different thickness (i.e., 20%, 40%, and 60%) with respect to the workpiece thickness was selected to assist the FSW joining at the plunge stage. It is observed that the downward force generated in the FSW process was gradually decreased after introducing Cu donor material with incremental thicknesses with respect to workpiece at the plunge stage. Post-weld analysis was characterized in terms of microstructure, and mechanical properties. The results of microstructure analysis at the stir zone (SZ) show the formation of finer grains due to dynamic recrystallization and plastic deformation. Micro-hardness tests reveal that the hardness decreased from the base metal (BM) to the SZ across the heat affected zone (HAZ) and thermo-mechanically affected zone (TMAZ). The lowest value of hardness appeared in the TMAZ and HAZ where tensile failure occurs. With increasing welding speed, the average hardness in the SZ decreased due to lower heat input and faster cooling rate. Tensile test plots show no significant change in ultimate tensile strength with or without Cu donor material. Fractography of tensile tested samples shows both ductile and brittle like structure for given welding parameters. This proposed work of FSW with Cu donor material is promising to increase tool life due to the decrement of the downforce during plunge and throughout the welding stage. Meanwhile, the inclusion of donor material did not compromise the weld quality in terms of the mechanical properties and micro-hardness.

What Is Your Main Contribution To The Field?

The main contribution in this research is on the novel and solid experimental approaches to examine whether donor material can assist friction stir welding (FSW) processes. To investigate this research question, Copper (Cu) was adopted as the donor material to assist the FSW of Al 6061. Through comparing experiments with and without donor material inclusion in FSW, it was found that the donor material induces drastic decreasing in downward force during FSW processes, which will increases the lifetime of the FSW tools. Meanwhile, the post-weld analysis identified no significant change occurred in the mechanical properties and microstructure of the welded joints, which is desired for industrial applications. The implementation of the donor material is promising to increase the lifetime of the FSW tools without compromising the mechanical properties FSW joints. The proposed approach is also economical for industrial application due to its effective potential to enhance the life of friction stir tools.

2. What is novel? In theory, in experimental techniques, or a combination of both?

This paper presents the novel experimental approach of introducing a Copper (Cu) donor material during the initial stage of friction stir welding. "Cu" was chosen as a donor material due to its high thermal conductivity property. This experimental technique generate friction heat quickly and soften materials in less time. Thus, it reduces downforce but still maintains properties in joints fabricated by FSW processes. This experimental approach is promising to improve friction stir tool life. The present experimental technique is unique and the theory/physics behind this approach is to understand thermo-mechanical mechanisms like frictional heat generation and conduction during welding.

3. Does your paper have industrial applications? If yes, who are the likely user?

The major applications of this paper is for aerospace, automotive, shipbuilding and railways industries. These industries commonly need to join parts made of Aluminium alloys, Magnesium alloys, Titanium alloys, and steels

that are hard to weld by conventional fusion welding. This paper provides the promising idea/approach to them on FSW applications of improving friction stir tool life without deteriorating the welded joints properties.

Introduction

Friction stir welding (FSW) is a novel solid-state joining process invented at The Welding Institute (TWI) of UK in 1991. It has been broadly used in aerospace, aircraft, shipbuilding, automotive, railways, and marine industries [1–4]. FSW has many advantages including lower heat input and avoidance evasion of phase change during the welding process in comparison to conventional fusion joining processes such as MIG or TIG welding. Since it is a solid state joining, this process does not cause material phase change, resulting in minimum microstructural changes and better mechanical properties than conventional welding processes [5–8]. NASA and aerospace manufactures are applying FSW to effectively and reliably join high-strength aerospace aluminum alloys such as Al 6061, Al 2024, and Titanium alloys that are hard to weld by conventional fusion welding. In the shipbuilding industry, FSW is used for joining high strength steel for hulls and decks.

A typical FSW process consists of four stages: plunge, dwell, welding, and retraction as shown in Fig. 1 (b). During the plunge stage, a non-consumable rotating tool's pin makes initial contact and penetrates the workpieces being joined. The plunge force and friction between the tool and the workpiece generate heat on the surrounding area of the tool, and result in viscous plastic deformation. The temperature keeps increasing, which softens the material to a paste-like state through thermo-mechanical deformation of the material around the pin. The axial load decreases and then enters the dwell stage. In the dwell stage, the tool shoulder establishes contact with the workpieces. During the dwell stage, the tool can no longer maintain a vertical displacement. It rotates in place until the surrounding material reaches a stabilized temperature for the welding stage. The length of the dwell time is decided by the properties of the workpiece material and the design of tool bit. The welding stage is the actual joining process of the workpieces. The rotating tool advances along a predefined welding path. As the tool moves along the welding path, viscous material is transferred from the advancing side (AS) of the pin to the retreating side (RS) and vice versa. As the tool passes along the welding path, the material cools and solidifies, resulting in a solid state joining of materials. The important control parameters in FSW are: rotation speed of the tool in rpm, traverse speed of the welding tool in mm/second, tilt angle, welding path, and tool design, etc. [9].

When applying the FSW in manufacturing of industrial parts, an issue hindering its wider application is that tool wear leads to high tooling cost when joining high strength materials such as steel and titanium alloys. The excessive wear in FSW results in frequent replacement of costly tools after an insufficient length of weld. The research team has proposed the idea of using donor materials in plunge stage to reduce the tool wear and increase tool life [10, 11, 12]. Due to equipment restriction, the previous research in [10–12] was performed on a manual mill; it only studied donor material's effect in the plunge stage of FSW. Through a literature research, there is no reported research that examined the effect of donor material on the welding stage and the joint properties of FSW. Initiated by these, a set of experiments were performed to study the Cu donor material in assisting FSW of Al 6061. The downward force, microstructure, mechanical properties, and micro-hardness in the Cu assisted FSW joining Al 6061 workpieces were examined at a combination of tool rotational rate of 1400 rpm and various welding speeds at 1 mm/s and 3 mm/s respectively. **These experiments aim to address the research question whether donor material can assist welding stage in FSW processes and affect post-weld properties.**

The rest of this paper is organized as follows. Section 2 reviews related research work on FSW process assisted by auxiliary energy and donor materials. A research gap is summarized at the end of this section. Section 3 discusses

the details of the proposed experimentation techniques. Section 4 describes experiment results and discussion to illustrate the physical mechanism of donor materials assisted FSW joints formation. Section 5 concludes the research and outlines future direction.

Literature Review

The related literature was searched on FSW assisted by various types of auxiliary energy and donor materials. Wu et al provided a comprehensive review [13] on the methods that provides auxiliary energy. These methods majorly are using electricity, induction, laser, and ultrasonic vibration etc., which partially heat and/or soften the alloys before or during the FSW, reduce the load requirement on the tool. Thus, it improves the tool performance and life, optimizes process window, and enhances welding efficiency and quality, etc.

Electrically assisted FSW (EAFSW) softens materials by Joule heating effect and electroplastic effect [14, 15]. Due to both effects, the EAFSW process produced significantly higher temperatures in the plunge stage to soften the material, which reduced the plunge force significantly [14, 15]. This would facilitate welding of thick part, improve the wear resistance of the tool, and increase the tool life and performance [14]. Luo et al applied EAFSW for joining light alloys of AZ31B and Al 7075 [16, 17]. Morphologies of the weld line in [16] confirmed smoother surfaces with finer arc shaped features due to more uniform and denser corrugation of the material. It was also reported that the influence of electric current would reduce the average grain size in the SZ [16]. Although the average grain size was almost unchanged in the TMAZ, the grain distribution was more uniform with more elongated grains due to severe plastic deformation. Also, it formed less narrow and more equiaxed grains in the TMAZ due to more severe dynamic recrystallization caused by electric current [16]. The difference in grain refinement in the SZ and TMAZ of the Al and Mg alloys is induced by the different responses of the alloys to nucleation rate of dynamic recrystallization under similar conditions of heat input and plastic deformation [17]. The higher is the nucleation rate of the dynamic recrystallization, the finer are the grains formed. The grains in the HAZ of EAFSW joints were coarsen with increasing electric current because of the long exposure of the HAZ to high temperature and secondary recrystallization. The hardness profiles of the EAFSW welds were consistent with the grain refinements and microstructure developments. The hardness values varied directly with the grain refinements. The higher heat inputs improved material flow. The viscoplasticity at the root of the weld improved the weld quality by reducing the risk of various defects in welds.

Induction assisted FSW (IAFSW) uses electrical inductance to generate heat to soften the workpiece materials. IAFSW has been reported for joining medium strength Aluminium alloy [18] and high strength steel [19, 20]. Both researchers in [18 and 19] reported that the downward force was reduced, but mechanical properties in the joints still maintained. Further, IAFSW would reduce the residual stress distortion and HAZ softening and increases the plastic deformation due to its low heat input flux and well defined heating. This would eliminate the heavy clamping systems thus reducing the size of the FSW machine [18]. When joining steel, the IAFSW, comparing to the FSW, process induced more intense grain refinement [19], which induced an increase in the hardness and tensile strength of the SZ. However, the ferrite/austenite ratio of this steel remained unchanged for both processes.

Laser assisted FSW (LAFSW) is the most widely used external energy assisted FSW. The application of laser preheating lowered the resistance of the material to tool penetration and forward motion [21]. Therefore, the need to apply large forces on both the tool and the workpieces is lowered. When applying EAFSW to high strength steel with ferrite pearlite structure, significant amount brittle Martensite and Bainite phases were found in the joints, but the LAFSW could prevent the brittleness [21] and retain the original phases. LAFSW was even applied for joining of

super alloys such as Inconel [22]. Laser preheat induced intense grain refinement in the SZ, so it significantly improved the overall strength and mechanical properties of Inconel alloy. An improvement was reported in the fatigue behavior of Aluminium lap joints produced by LAFSW [23]. Alvarez et al. also reported the life of a PCBN tool used in the LAFSW of marine grade steel was increased up to several feet [20].

Ultrasonic energy assisted FSW (UAFSW) uses high frequency vibration to soften material without significant heating it. UAFSW reduces the friction heat by complementing the softening. However, at the same time, it would increase the heat generation from the additional deformation. The overall result of these two effects may increase the heat input slightly. UAFSW expanded the plastically deformed region [24] and improved the material flow [25], thus it improved lap shear force and hardness of the joints [25]. UAFSW also suppressed the formation of voids and tunnel defects [24, 26].

Numerical [10–12] and experimental [11–12] studies of donor materials that assisted FSW suggest that local preheating at the plunge stage is generated by friction between the tool pin and the donor material and also by the plastic deformation in the material. This preheating would generate heat in the copper donor material due to high frictional forces and this preheating is expected to be transferred to the work piece by conduction, which will result in softening the workpiece material and reducing the plunge force. This in turn is expected to reduce tool wear. For the selection of a donor material, it is desired for the donor material to possess high thermal conductivity to allow rapid heat transfer into the workpiece. Additionally, it is desired that the donor material will not advance along the welding path, because this will influence the weld quality by producing a nonhomogeneous weld line. It has been demonstrated by previous studies that material moves around the tool pin and becomes deposited behind it without being transported forward with the tool's pin [27–29]. Hence, donor material from the plunge phase is restricted to the initial weld area and can be sacrificed.

Comparing to the auxiliary energy assisted FSW, the donor material assisted FSW does not require the welding tool to be electrically conductive, and it needs no installation of complex insulation system between the tool and the FSW machine. It also avoids the difficulty in IAFSW on controlling the current flow, generating the spark, and heating of conductive materials involved in the current path. It also avoids the complex equipment for laser and ultrasonic energy. This donor material assisted FSW idea is unique. Except the paper [10–12] on examining the plunge stage, there is no reported work examining the effect of donor material on the welding stage and the joint properties of FSW. To fill this gap, the proposed methodology is presented in Sect. 3.

Experimental Procedure

The selected base metal in this study was an extruded 6.35 mm thick AA6061-T6 aluminum alloy which is a commonly used light weight metal in aerospace applications. The AA6061 comes in sheet form with dimensions of 317.5 mm (length) × 76.2 mm (width). Cu 110 was selected as the donor material due to its high thermal conductivity. The chemical composition and mechanical properties of the selected materials are listed in Tables 1, 2, and 3 respectively.

Table 1
Chemical composition of AA6061-T6 alloy

Components	Al	Cr	Cu	Fe	Mg	Mn	Ni	Si	Ti	Zn	Zr	Others
Wt. %	95.1– 98.2	0.4– 0.8	0.05– 0.4	0– 0.7	0.8– 1.2	0– 0.15	0– 0.05	0.4– 0.8	0– 0.15	0– 0.25	0– 0.25	0.15

Table 2
Chemical composition of Cu 110 alloy

Components	Cu	Bi	Pb	O
Wt. %	99.9	0-0.005	0-0.005	0-0.04

Table 3
Mechanical properties of Cu 110 and AA6061-T6

Materials	Hardness (Rockwell)	Yield strength, MPa	UTS, MPa	Thermal conductivity, W/mK	Melting Point, °C
Copper 110	55	255	345	183	1084
Al 6061	40 (scale A), 60 (scale B)	241	262	151	585

Test coupons, with dimensions of 152.4 mm (length) × 76.2 mm (width), were sectioned from the as-received plates followed by milling the edges along the length as shown in Fig. 2 (a). An aperture of 63.5 mm (length) × 25.4 mm (width) is created to anchor the stir donor material to the workpiece through set screws. The aperture and the donor material were cut using a Haas CNC mill prior to the welding as shown in Fig. 2 (b-c). The Cu donor material thickness for the present investigation was set at 20%, 40%, and 60% of the depth of the workpiece thickness.

Prior to FSW, the workpiece surfaces and surrounding areas were cleaned using ethanol followed by scouring with an abrasive pad to remove oxides and debris. Finally the workpieces were cleaned again with ethanol. The workpieces were then tightly clamped using a welding fixture that was secured to the back anvil/worktable of the FSW machine. FSW experiments were conducted in position control mode with a triangular tapered pin-type H13 steel tool head. The shoulder's diameter was 15.8 mm with an adjustable 1/2–16 left-hand threaded pin having a diameter of 6.4 mm, a threaded length of 6.35 mm, a 60-degree thread at 1 mm pitch and 0.4 mm depth (normal to the surface). The tool-to-workpiece angle was maintained at 2° with a shoulder heel plunge depth (the portion of the shoulder under the top surface of the workpiece) of approximately 0.5 mm for all the welding experiments. The welding direction was parallel to the extruded direction of the workpiece (Fig. 1(a)). All the joints were friction stir welded at a speed of 1 mm/s or 3 mm/s. The tool rotational rate was kept constant at 1400 rpm and a penetration depth of 5.85 into the workpieces. It is noted that relative to the welding and tool rotational directions as indicated in Fig. 1(a), the welds were joined with the counter-clockwise tool rotation. The final friction stir welded aluminum plates are shown in Fig. 2(d). The weld properties were examined in terms of microstructure, Vickers micro-hardness, tensile test, and fractography. For each friction stir welded assembly, the unstable (ramp up and ramp down) regions at the beginning (~ 20 mm) and end (~ 20 mm) of the weld line were removed. Using a precision wire electrical discharge machine (EDM), the FSWed assemblies were sectioned into samples in the direction perpendicular to the welding direction (WD) for microstructure characterization and for conducting tensile test experiments in the weld cross-sections. Sectioned samples were then cold mounted, ground and polished with different grades of emery sheets, and a final polishing with 0.05 μm grit cloth. The samples were then etched with a standard Keller's reagent [190 mL H₂O, 5 ml HNO₃, 3 ml HCl, and 2 mL HF] for approximately 120 seconds to reveal the grain structure.

The metallographic analyses were accomplished using an Olympus optical microscope equipped with quantitative image analysis software for microstructure and macrostructure studies, respectively. Automated Vickers micro-hardness measurements were conducted across the welded cross-sections using a load of 100 g, a dwell time of

15 seconds, and an indent interval of 0.3 mm (i.e., at least three times the diagonal length of the indentation to prevent any potential effect of the strain fields caused by adjacent indentations). The tensile tests experiments were carried out by a universal tensile testing machine (INSTRON-5869) with a 50kN load capacity. At least two samples were tested at each welding condition. Tensile samples were prepared according to ASTM E8/E8M-13a [30]. All tensile tests were performed up to failure at room temperature and at a crosshead speed of 1.5 mm/min. The fractured surface of the frictionally stir welded (FSWed) samples subsequent to the tensile testing was examined using a JEOL 6700 field effect-scanning electron microscope (FE-SEM) equipped with three-dimensional (3-D) fractographic analysis capacity.

Results And Discussion

4.1 Downward force generation

The downward force is a significant parameter, which influences the joint quality and tool life during the plunge and welding stages. A load cell with a National Instrument Data Acquisition (NI-DAQ) device were used to collect the force data in the joining experiment. Figure 3 (a-b) demonstrates the downward force produced at a constant 1400 rpm tool rotational speed and welding speeds of 1 mm/s and 3 mm/s on different donor material thickness settings, respectively. It can be noticed from the plots of Fig. 3(a-b) that the downward force in the aforementioned plunge, dwell, welding and retraction stages shows the following trend. During plunge stage the rotating tool approaches the surface of the workpiece and penetrates into the workpiece generating initial frictional heat. At this point the downward force starts to increase and reaches to the peak position until to the end of plunge stage. Thereafter, in the dwell stage the downward force begins to drop gradually, which indicates that the required operating temperature is achieved to weld the workpiece. In the welding stage, the constant frictional energy generates high temperatures which soften the workpiece, at this point the downward force keeps stable and increased slightly until it reaches to the exit position, then it immediately reduced to zero downward force in the retraction stage. It is understandable that the higher downward forces were taking place during the plunge stage which resulted in producing frictional heat that softened the surrounding material [31–32]. Several authors [33–34] also reported similar findings on friction stir welding of aluminum alloys. They also observed that the downward force increases during the initial plunge stage and then suddenly drops with further advancement of the tool head. It was observed that with the embedded donor material at the initial plunge stage, the downward force decreases significantly as the donor material thickness increases by 20%, 40%, and 60% of the workpiece material. In Fig. 3 (a-b), the downward force variation with time is compared for the as-received welded sample and the donor material welded ones.

The downward force obtained during the plunge stage for the welding speed of 1mm/s and tool rotational rate of 1400 rpm was much higher; it reached approximately 8kN for an as-welded (AW) sample, 12 kN for 20%, 8 kN for 40%, and 7.5 kN for 60% Cu donor material assisted sample. As compared to the plunge stage, during the welding stage, the downward force was predominantly reduced by 83%, 66%, and 40.6% when the donor material was 60%, 40%, and 20% of the workpiece samples respectively. Similarly, during the plunge stage at a welding speed of 3mm/s and tool rotational rate of 1400 rpm, the downward force reached approximately 8.75 kN, 7.5 kN, and 6 kN for the 20%, 40%, and 60% Cu donor material respectively.

During the welding stage, the downward force fluctuates between 2.5 kN to 3.75 kN for 20%, 40%, and 60% donor material. There was no significant difference noticed in the downward force during the welding stage of the aluminum plates with or without the donor material for the 3 mm/s welding speed. This could be due to lack of

generating enough heat during the initial plunge stage to soften the surrounding material in addition to a faster cooling rate. Therefore, it is evident that plunging through the Cu donor material generates frictional heat that transfers to the aluminum workpiece that further softens the aluminum workpiece. The use of a donor material concept in preheating the workpiece could further help in selecting proper welding conditions and also in producing optimal welds.

4.2 Microstructure

The thermo-mechanical condition change in FSW leads to form different regions in the welding location: namely the SZ or weld nugget around the weld center, the TMAZ and the HAZ on advancing and retreating sides of the weld and the BM. These regions are shown in Fig. 4 (a-e, where the typical microstructures were observed across a weld made at 1 mm/s welding speed and 1400 rpm tool rotational rate. Similar observations have been documented by others [35–36]. It is generally believed that the material in FSW undergoes continuous and discontinuous dynamic recrystallization [6, 28, and 36], grain refinement, and grain coarsening. In the SZ (Fig. 4(b)), a severe plastic deformation and the elevated temperature led to dynamic recrystallization of the AA6061-T6 alloy plates. The grains became predominately equiaxed in both the AS and the RS respectively. The grains in the SZ were smaller and equiaxed as compared to the grains in the BM, suggesting that the current selected FSW assisted donor material conditions resulted in grain refinement. In the TMAZ, the microstructure was highly deformed and grains appeared to be distorted, and elongated. The dynamic recrystallization process did not fully develop in TMAZ during FSW experiment.

The HAZ microstructure which falls between the BM and the TMAZ is mostly experiencing the effect of frictional heating and no interference of mechanical forces. This leads to partial recrystallization of the larger grains in the BM microstructure. Figure 5 shows images of the microstructures of selected regions within the SZ obtained at 20%, 40%, 60% Cu donor material and as-welded condition. At the SZ weld location, there is no significant change in grain growth observed both with or without donor material as clearly seen in Fig. 5 (a-d). This could be due to the rapid dissipation of the heat generated during the plunge stage throughout the workpiece surrounding area.

4.3 Micro-hardness

Vickers micro-hardness profiles were generated at the top, mid, and bottom layers of the workpiece across the weldments with different welding parameters and different donor material thicknesses as shown in the Fig. 6 (a-b). The indentation hardness is measured starting from the BM advancing side to the BM retreating side. It is observed that the hardness profiles exhibited a W-shape. From the plotted hardness profiles in Fig. 6, it was noticed that the RS of the weld closer to the tool pin had lower hardness compared to the AS, this is due to strains developed in the workpiece by the welding tool. The temperature during FSW on the AS side is higher than on the RS side, which enhances the hardness on the AS side.

The minimum hardness occurred at the HAZ with HV values of about 65–68 and it rose up to HV values of 80–85 at the SZ. The highest hardness values of HV of 100–110 occurred in the BM zone. The average minimum hardness in the SZ was equivalent to 77 % of the base metal. The hardness in the SZ also depends on the precipitation distribution since the AA6061-T6 is a precipitation hardened alloy [37]. The hardness values in the SZ were higher than in the TMAZ and the HAZ, due to dynamic recrystallization and grain refinement as discussed above in the microstructure section. In the HAZ, the material undergoes only softening, the hardness observed were the lowest in each weld. There is no intense plastic deformation and grain refinement in the HAZ, which is evident from the grain coarsening.

The TMAZ undergoes some plastic deformation with addition of heating; this leads to grain refinement compared to the HAZ. Therefore, it was found that higher hardness values occurred in the TMAZ as compared to the HAZ due to strain hardening. With increasing Cu donor material thickness, the heat input and peak temperature increase. Thus, it further accelerates the dissolution, precipitation, and growth of secondary phases. According to [38–39], this grain refinement at SZ and HAZ is mainly attributed to the dissolution and precipitation of secondary phases and change in microstructure of the weld zone. The increase in the hardness in the SZ is due to severe plastic deformation and dynamic recrystallization with the donor material inserted on top of the workpiece during the plunge stage. With the amount of heat generated by friction between the tool head and the donor material, the grain refinement predominantly occurred in the SZ. This led to increased hardness inside the SZ. It is noted that the hardness in the SZ, the TMAZ, and the HAZ with 20% Cu donor material is higher than that of the 60% Cu stir donor material and also of the Al-Al control welded samples with 3 mm/s welding speed. This is due to slower cooling rate in the 20% Cu donor samples, which led to the SZ to retain most of its heat for a longer period which resulted in added hardness of the material. During microstructural analysis, it was observed that the grain refinement has taken place in the order of SZ < TMAZ < HAZ < BM, with average grain size of 4.77 μm in the SZ, 9.6 μm in the TMAZ, 56.73 μm in the HAZ, and 83 μm in the BM. Since the AA6061 is a heat treatable alloy, the precipitations of Mg₂Si in Al 6061 are responsible to enhance the strength of the alloy [40]. Several investigations have demonstrated that the hardness of the aluminum alloys was mostly affected by precipitate distribution rather than grain size [41]. These precipitates highly dissolve in FSW processes, which eventually reduces the UTS of FSW joints. The changes in hardness distribution at different zones could be due to high dissolution of the precipitate and grain size during FSW [42–43].

4.4 Tensile test

Figure 7 (a-b) shows comparison of tensile test properties of joints made at 1400 rpm tool rotational speed and welding speeds at 1 mm/s and 3 mm/s respectively. The ultimate tensile strength (UTS) of the FSWed samples were found to be less than the base material. The average UTS for AW control samples obtained at 1400 rpm and 1 mm/s was 192 MPa. Using the same rotational and welding speed, the average UTS of the 20%, 40%, and 60% donor assisted FSW joints was similar to the AW samples of ~ 190 MPa. For the joints made at 1400 rpm and 3 mm/s, the average UTS of AW samples decreases to 180 MPa. The UTS values were 187 and 166 MPa for the 60% and 20% donor assisted samples respectively. It was also observed that the ductility decreased constantly from Al-Al to 20%, 40%, and 60% Cu donor material at 1400 rpm, 3 mm/s welding conditions. This ductility loss is due to secondary cracks generated in the metal matrix during welding. The amount of heat loss is more due to faster cooling rate and lower heat input is less in 3 mm/s welding speed.

Fig. 7 (c-d) shows the failure location of joints produced at 1400 rpm with a speed of 1 mm/s and 3 mm/s respectively. All samples were fractured on the RS side near the TMAZ/HAZ in conjunction with the micro-hardness profiles where the lowest hardness occurred in the HAZ location. The HAZ location is the weakest zone of the welded samples. He et al. [41] also reported similar fracture locations subsequent to tensile testing in FSW joint made of thick AA6061-T6 plates. The nature of the fractured surface appeared to be ductile with dimple-like structures. It was noticed that the donor material did not impact the UTS of the joints for the of 1400 rpm and 1 mm/s tested samples. However, the joints of the welded samples at 1400 rpm and a speed of 3 mm/s were found to have some secondary cracks and tear ridges, which led to a combination of brittle and ductile fracture as shown in Figure 9. These preexisting secondary cracks sites are the easiest location where crack initiation starts internally and cause rapid failure during the tensile testing. The tensile fracture starts at the HAZ location in a brittle fashion

and propagates at 45° into the TMAZ/SZ in a ductile fashion. This can be seen in the images shown in Fig. 7 (c) and (d).

4.5 Fractography

Fractured surfaces of all tensile samples were investigated by field emission scanning electron microscope (FE-SEM). Figure 8 (a-h) shows the fracture morphologies of the 1400 rpm and 1 mm/s welded samples. These fractographic images consist of crack initiation, spherical and broken dimples, secondary cracks, tear ridges, and particles. It has been observed that crack initiation occurs near the TMAZ/HAZ on the RS. The fractured surface presents large number of small spherical dimples with layered distribution, which often belongs to a ductile fracture. The fractured surface is covered with small deep dimples embedded with secondary particles which indicates good ductility. In higher magnification, dimples are clearly visible in images as shown in Fig. 8 (b, d, f) and Fig. 9 (a, e, g). These dimples appear in the ductile fractured surface, which are only corresponding to a void. The failure mode was observed to be ductile fracture in AW with 20%, 40%, and 60% donor material. However, there were also some tearing ridges seen on the fractured surface which indicates loss of ductility.

Fig. 9 (a-i) shows fracture morphologies of the 1400 rpm with a speed of 3 mm/s welded sample. These fractographic images consist of crack initiation, spherical and broken dimples, secondary cracks, tear ridges, and secondary phase particles. In the AW fractured surface, the secondary phase particles were embedded in the dimples which indicates good ductility. This can be observed in the tensile test plots Fig. 7 (b). The secondary cracks and broken dimples are observed on all fracture surfaces which indicates brittle fracture and lost ductility in comparison with AW condition. This loss of ductility can be clearly seen in Fig. 7 (b). All these features indicate that a combination of brittle and ductile fractures was observed in the 20%, 40%, and 60% Cu donor materials assisted FSW.

Conclusions And Future Work

In this study, Cu donor material assisted FSW was successfully used in the joining of AA6061-T6 alloy plates using different welding speeds and a constant tool rotational speed. The downward force, post-weld microstructure and mechanical properties of the welded plates were studied. The following important conclusions are drawn from this study.

1. The downward force generated in the FSW processes gradually decreased subsequent to embedding the Cu donor material by 20%, 40%, and 60% of the workpieces. The downward force is decreased by a maximum of 83% for a 60% Cu donor material due to excessive heat transfer from the donor material to the workpiece. This proposed work of integrating a Cu donor material at the initial plunge stage is promising to increase the tool life without compromising the mechanical properties for the given welding parameters. The implementation of the donor material increases the lifetime of the FSW tools which is critically useful and economical.
2. The stir zone (SZ) and the thermo-mechanically affected zone (TMAZ), which were predominantly composed of equiaxed grains, experienced full dynamic recrystallization. The grain size in the SZ decreased with an increasing heat input (i.e., increasing tool rotational rate and decreasing welding speed). The average grain size in the SZ is 4.77 μm , the TMAZ is 9.6 μm , the HAZ is 56.73 μm , and the BM is 83 μm . There was no change in grain size in the SZ with embedded Cu donor material for the different thicknesses of the workpiece used in this research (20%, 40%, and 60%).

3. The joints presented a W-shaped hardness profile the their cross-section. The minimum hardness of HV 65–68 was measured in the HAZ and increased to a HV of 80–85 at the center of SZ. When the welding speed was increased from 1 mm/s to 3 mm/s, the measured hardness of the HAZ gradually decreased whereas the hardness in the SZ increased. The overall measured hardness across the SZ was slightly higher at a lower heat input (i.e., at a constant tool rotational rate and/or a higher welding speed).

4. The maximum tensile strength obtained at 1400 rpm and 1 mm/s was 192 MPa for both with and without Cu donor material, which is 73.2% of the base material. The joints made with Cu donor material had no significant effect on the improvement of the tensile strength.

5. Fractography of the tensile testing failure samples for the 1400 rpm, 1 mm/s joints exhibited ductile like fracture with some secondary particles in addition to spherical and broken dimples. The fractured surface for the 1400 rpm, 3 mm/s speed appeared to be a combination of brittle and ductile like fracture. The secondary cracks and broken dimples were also observed for the 20%, and the 60% Cu donor material.

In summary, although it is proven that the downward force is drastically decreased with embedded Cu donor material, no significant changes occurred in the mechanical properties of the welded joints. In the future, to further understand the temperature profiles and enhance the mechanical properties, the authors will continue to conduct further testing and measurement of the temperature profiles at different welding regions and conduct heat treatment with several solution treatment and aging time limits.

Declarations

Acknowledgements

The authors would like to acknowledge support from NASA (award number: 80NSSC20M0015). Any opinions, findings, and conclusions or recommendations expressed in this material are those of the author(s) and do not necessarily reflect the views of the NASA. The authors would also like to thank the Commonwealth Center for Advanced Manufacturing (CCAM) and Amsted Rail for providing the facility for sample characterization. The assistance of Geoff Widman in performing the experiments is also gratefully acknowledged.

- a. Funding:** The work is supported by NASA (award number: 80NSSC20M0015). Any opinions, findings, and conclusions or recommendations expressed in this material are those of the author(s) and do not necessarily reflect the views of the NASA.
- b. Conflicts of interest/Competing interests:** The authors have no conflicts of interest to declare that are relevant to the content of the article.
- c. Availability of data and material (data transparency):** Data is available upon request. We will also deposit it to a repository after acceptance.
- d. Code availability:** Not applicable
- e. Ethics approval:** Not applicable. This research is on FSW experimentation, it does not need Institutional Review Board (IRB) approval.
- f. Consent to participate:** Not applicable
- g. Consent for publication:** The authors give our consent for the publication of identifiable details, which can include photograph(s) and details within the text (“Material”) to be published in the International Journal of

h. Authors' contributions: Dr. S. Bhukya carried out experimentation and data analysis, and wrote/revised the manuscript. Dr. Z. Wu, as the Principal Investigator, secured funding and resources for the research, designed experiment, wrote and revised the manuscript. Mr. J. Maniscalco carried out FEA simulation of the experiment and proofread the manuscript. Dr. A. Elmoustafa conceptualized the experiment, reviewed and revised the manuscript.

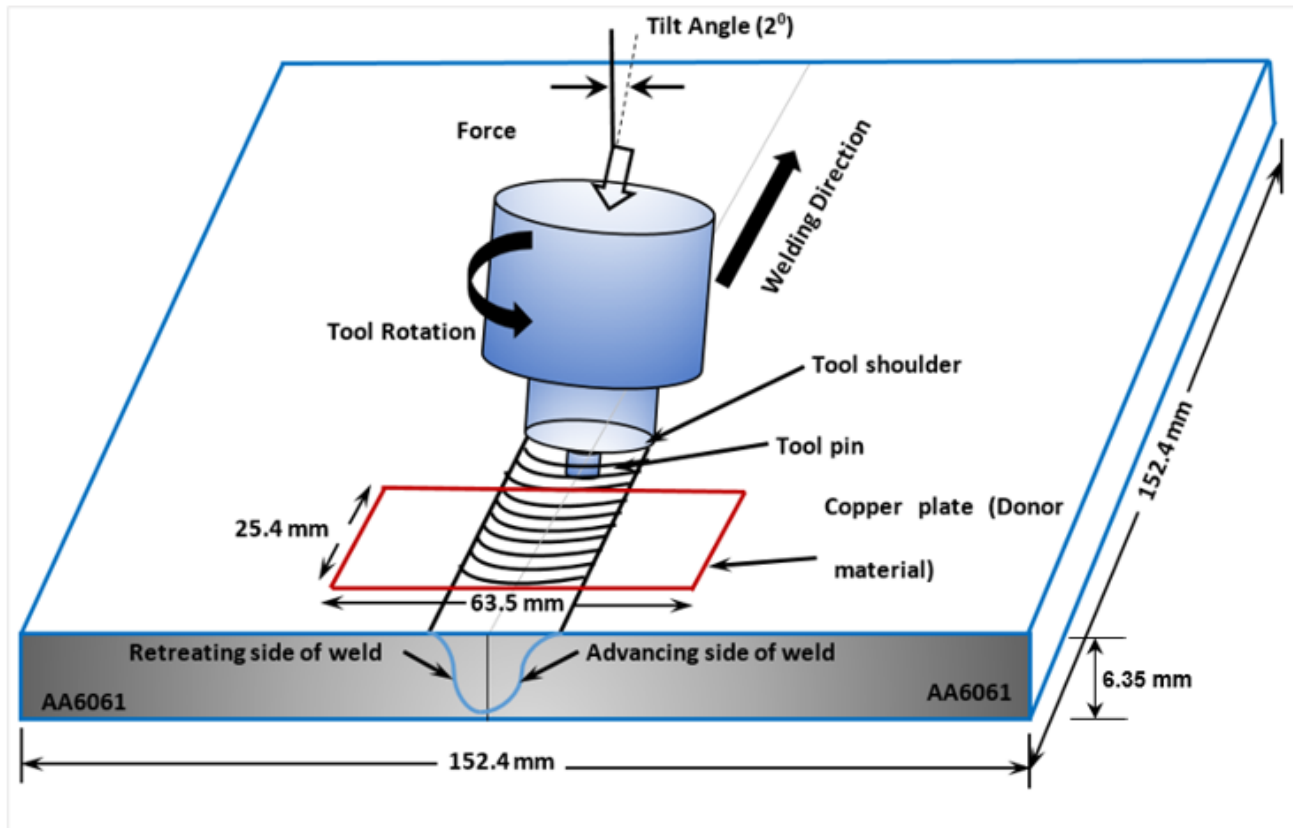
References

1. Thomas WM, Nicholas ED, Needham JC, Murch MG, Templesmith P, Dawes CJ, et al. Patent Application No. 9125978.8;1991.
2. Zhao J, Jiang F, Jian HG, Wen K, Jiang L, Chen XB. Comparative investigation of tungsten inert gas and friction stir welding characteristics of Al–Mg–Sc alloy plates. Mater Des 2010;31:306–11.
3. Cavaliere P, Cabibbo M, Panella F, Squillace A. 2198 Al–Li plates jointed by friction stir welding: mechanical and microstructural behavior. Mater Des 2009;30:3622–631.
4. Thomas WM, Nicholas ED. Friction stir welding for the transportation industries. Mater Des 1997;18:269–73.
5. Mishra RS, Ma ZY. Friction stir welding and processing. Mater Sci Eng R 2005;50:1–78.
6. Bousquet E, Poulon-Quintin A, Puiggali M, Devos O, Touzet M, Relationship between microstructure, microhardness and corrosion sensitivity of an AA 2024-T3 friction stir welded joint, Corrosion Science 2011;53:3026-34.
7. Ericsson M, Sandström R, Influence of welding speed on the fatigue of friction stir welds, and comparison with MIG and TIG, International Journal of Fatigue 2003;25: 1379-87.
8. M. Jariyaboon, A.J. Davenport, R. Ambat, B.J. Connolly, S.W. Williams, D.A. Price, The effect of welding parameters on the corrosion behaviour of friction stir welded AA2024-T351, Corrosion Science, 49 (2007) 877-909.
9. Rice JM, Mandal S, Elmoustafa AA. Microstructural investigation of donor material experiments in friction stir welding. Int J Mater Form 2014;7:127–37.
10. Mandal S, Rice J, Hou G, Williamson KM, Elmoustafa AA. Modeling and simulation of a donor material concept to reduce tool wear in friction stir welding of high-strength materials. J Mater Eng Perform 2013; 6:1558–564.
11. Mandal S, Rice J, Elmoustafa AA. Experimental and numerical investigation of the plunge stage in friction stir welding, J Mater Process Technol 2008;23:411-19.
12. Mandal S. Numeric/Experimental Investigation of Plunge Stage and Effect of Donor Material in Friction Stir Welding, Ph.D. Dissertation, Old Dominion University, Norfolk, 2009.
13. G. K. Padhy, C. S. Wu, and S. Gao, Auxiliary energy assisted friction stir welding – status review, Science and Technology of Welding and Joining, 2015, Vol 613, No 8, 631-649
14. H. Potluri, J. J. Jones and L. Mears: 'Comparison of electrically assisted and conventional friction stir welding processes by feed force and torque'. Proc. ASME 2013 Int. Manufacturing Science and Engineering Conf., Madison, WI, USA, June 2013, ASME, paper MSEC2013-1192.
15. X. Liu, S. Lan and J. Ni: 'Electrically assisted friction stir welding for joining Al 6061 to TRIP780 steel', J. Mater. Process. Technol., 2015, 219, 112–123.
16. J. Luo, W. Chen and G. Fu: 'Hybrid-heat effects on electrical current aided friction stir welding of steel, and Al and Mg alloys', J. Mater. Process. Technol., 2014, 214, 3002–3012.

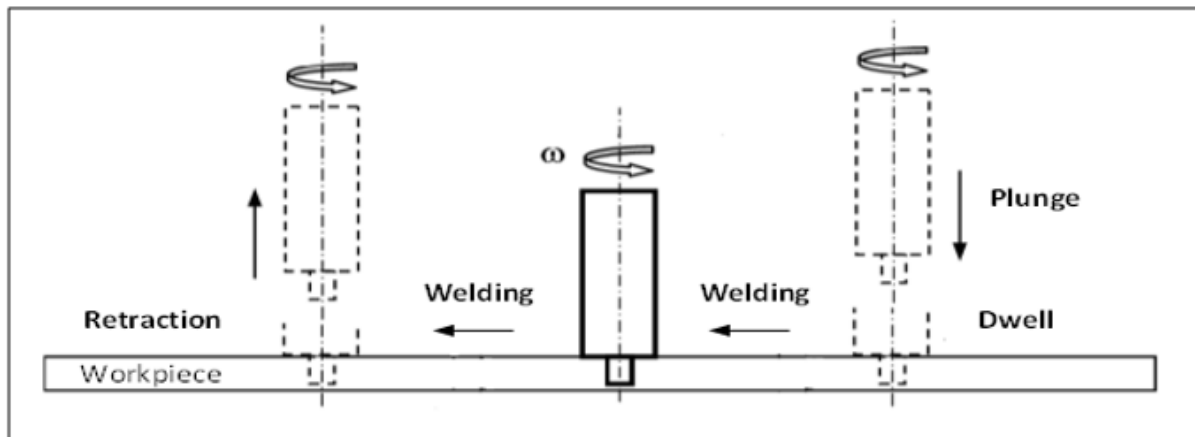
17. J. Luo, F. Li and W. Chen: 'Experimental researches on resistance heat aided friction stir welding of Mg alloy', *Q. J. Jpn Weld. Soc.*, 2013, 31, 65s–68s.
18. G. Oeystein, K. A. Ove, O. T. Midling and N. Hydro: 'Modified friction stir welding', International patent application no. WO1999039861 A1, August; 1999.
19. I. Alvarez, M. Garcia, G. Pena, J. Sotelo and D. Verdera: 'Evaluation of an induction-assisted friction stir welding technique for super duplex stainless steels', *Surf. Interface Anal.*, 2014, 46, 892–896.
20. I. Alvarez, V. Cid, G. Pena, J. Sotelo and D. Verdera: 'Assisted friction stir welding of carbon steel: use of induction and laser as preheating techniques', 1st edn, Vol. 7, in 'Friction stir welding and processing VII', (ed. R. Mishra et al.), 117–126; 2013, Warrendale, PA, TMS (The Minerals, Metals & Materials Society), John Wiley and Sons.
21. Y. F. Sun, Y. Konishi, M. Kamai and H. Fujii: 'Microstructure and mechanical properties of S45C steel prepared by laser-assisted friction stir welding', *Mater. Des.*, 2013, 47, 842–849.
22. K. H. Song, T. Tsumura and K. Nakata: 'Development of microstructure and mechanical properties in laser-FSW hybrid welded Inconel 600', *Mater. Trans.*, 2009, 50, 1832–1837.
23. S. L. Campanelli, G. Casalino, C. Casavola and V. Moramarco: 'Analysis and comparison of friction stir welding and laser assisted friction stir welding of aluminum alloy', *Materials*, 2013, 6, 5923–5941.
24. X. C. Liu, C. S. Wu and G. K. Padhy: 'Improved weld macrosection, microstructure and mechanical properties of 2024Al-T4 butt joints in ultrasonic vibration enhanced friction stir welding', *Sci. Technol. Weld. Join.*, 2015, 20, 345–352.
25. Y. Rostamiyan, A. Seidanloo, H. Sohrabpoor and R. Teimouri: 'Experimental studies on ultrasonically assisted friction stir spot welding of AA6061', *Arch. Civ. Mech. Eng.*, 2015, 15, 335–346.
26. L. Shi, C. S. Wu and X. C. Liu: 'Modeling the effects of ultrasonic vibration on friction stir welding', *J. Mater. Process. Technol.*, 2015, 222, 91–102.
27. Zhao YH, Lin SB, Qu FX, Wu L. Influence of pin geometry on material flow in friction stir welding process, *Mater Sci Technol* 2006; 22(1):45-50.
28. Seidel TU, Reynolds AP. Visualization of the material flow in AA2195 friction stir welds using a marker insert technique. *Metall Mater Trans A* 2001; 32:2879–884.
29. Guerra M, Schmidt C, McClure JC, Murr LE, Nunes AC, Flow patterns during friction stir welding. *Mater. Charact* 2003;49:95–101.
30. ASTM E8/E8M-13a. Standard Test Methods for Tension Testing of Metallic Materials; ASTM International: West Conshohocken, PA, USA, 2013.
31. Astarita A, Squillace A, Carrino L. Experimental study of the forces acting on the tool in the friction-stir welding of AA 2024 T3 sheets. *J Mater Eng Perform* 2014;23(10):3754-61.
32. Zimmer S, Langlois L, Laye J, Bigot R. Experimental investigation of the influence of the FSW plunge processing parameters on the maximum generated force and torque. *Int J Adv Manuf Technol* 2010;47:201-15.
33. Banik A, Barma JD, Saha SC. Effect of threaded pin tool for friction stir welding of AA6061-T6 at varying traverse speeds: torque and force analysis. *Iran J Sci Technol Trans Mech Eng* 2020;44:749-64.
34. Lambiase F, Paoletti A, Di Ilio A. Forces and temperature variation during friction stir welding of aluminum alloy AA6082-T6. *Int J Adv Manuf Technol* 2018;99:337-46.
35. Cam G. Friction stir welded structural materials: beyond Al-alloys. *Int Mater* 2011; Rev 56:1–48.

36. Sato Y S, Kokawa H, Enomoto M, Jogan S. Microstructural evolution of 6063 aluminum during friction-stir welding. *Metall Mater Trans A* 1999;30:2429–437.
37. Su JQ, Nelson TW, Sering CJ. Microstructure evolution during FSW/FSP of high strength aluminum alloys. *Mater Sci Eng A* 2005;405:277–86.
38. Li YP, Sun DQ, Gong WB, Liu, L. Effects of postweld aging on the microstructure and properties of bobbin tool friction stir-welded 6082-T6 aluminum alloy. *Int J Miner Metall Mater* 2019;26:849–57.
39. Li WY, Fu T, Hütsch L, Hilgert J, Wang FF, dos Santos JF, Huber N. Effects of tool rotational and welding speed on microstructure and mechanical properties of bobbin-tool friction-stir welded Mg AZ 31. *Mater Des* 2014;64:714–20.
40. Lin H, Hwang JR, Fung CP. Fatigue Properties of 6061-T6 Aluminum alloy butt joints processed by vacuum brazing and tungsten inert gas welding. *Advances in Mech Engg* 2016;8:1–13.
41. He J, Ling Z, Li H. Effect of tool rotational speed on residual stress, microstructure, and tensile properties of friction stir welded 6061-T6 aluminum alloy thick plate. *Int J Adv Manuf Technol* 2016;84:1953–961.
42. Sato Y S, Kokawa H, Enomoto M, Jogan S, Hashimoto T. Precipitation sequence in friction stir weld of 6063 aluminum during aging. *Metall Mater Trans A* 1999;30:3125–130.
43. Sato Y S, Kokawa H, Ikeda K, Enomoto M, Hashimoto T, Jogan S. Microtexture in the friction-stir weld of an aluminum alloy. *Metall Mater Trans A* 1999;32:941–48.

Figures



(a)



(b)

Figure 1

Schematic Illustration of (a) FSW Process, (b) Stages of FSW

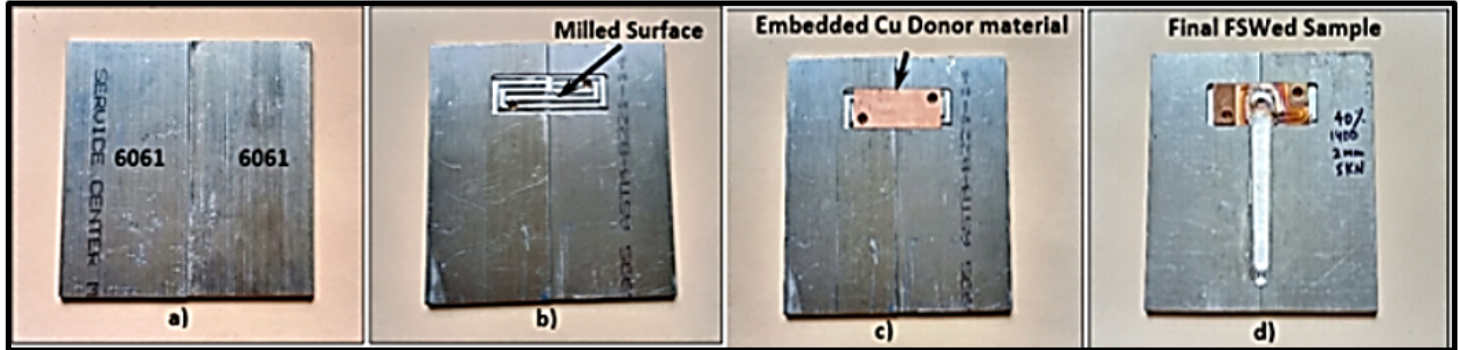


Figure 2

Steps for making FSW samples.

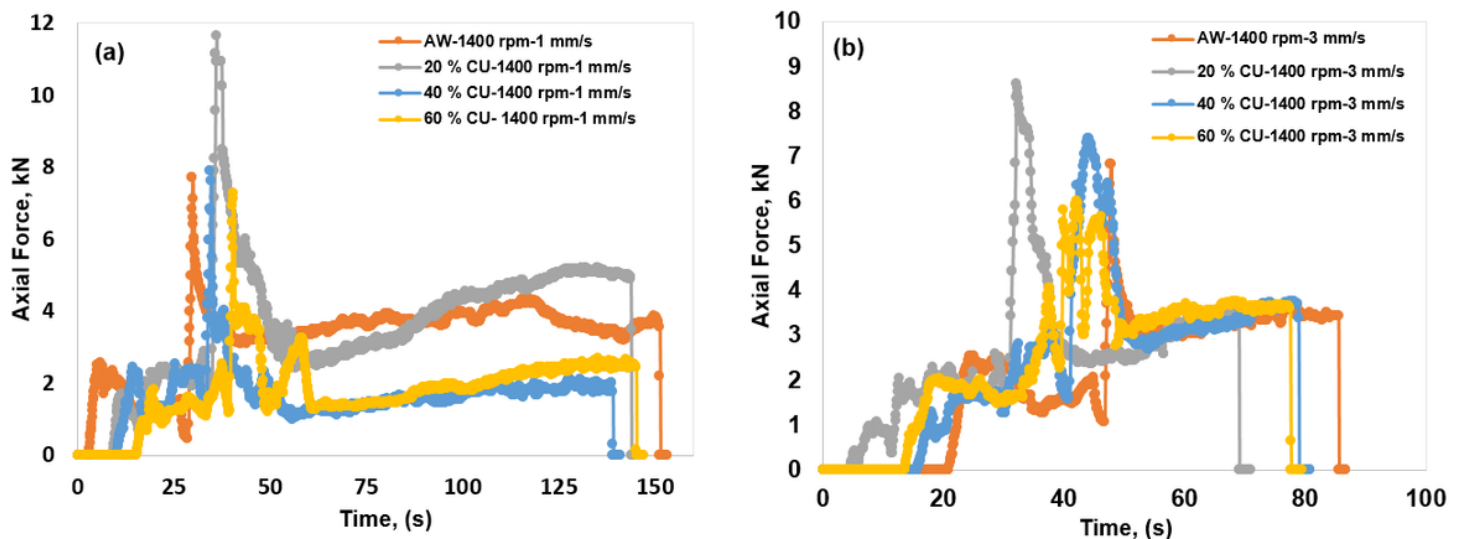


Figure 3

Downward Force vs time during welding process with and without Cu donor material at a tool rotational speed of 1400 rpm and welding speeds of (a) 1mm/s, (b) 3 mm/s.

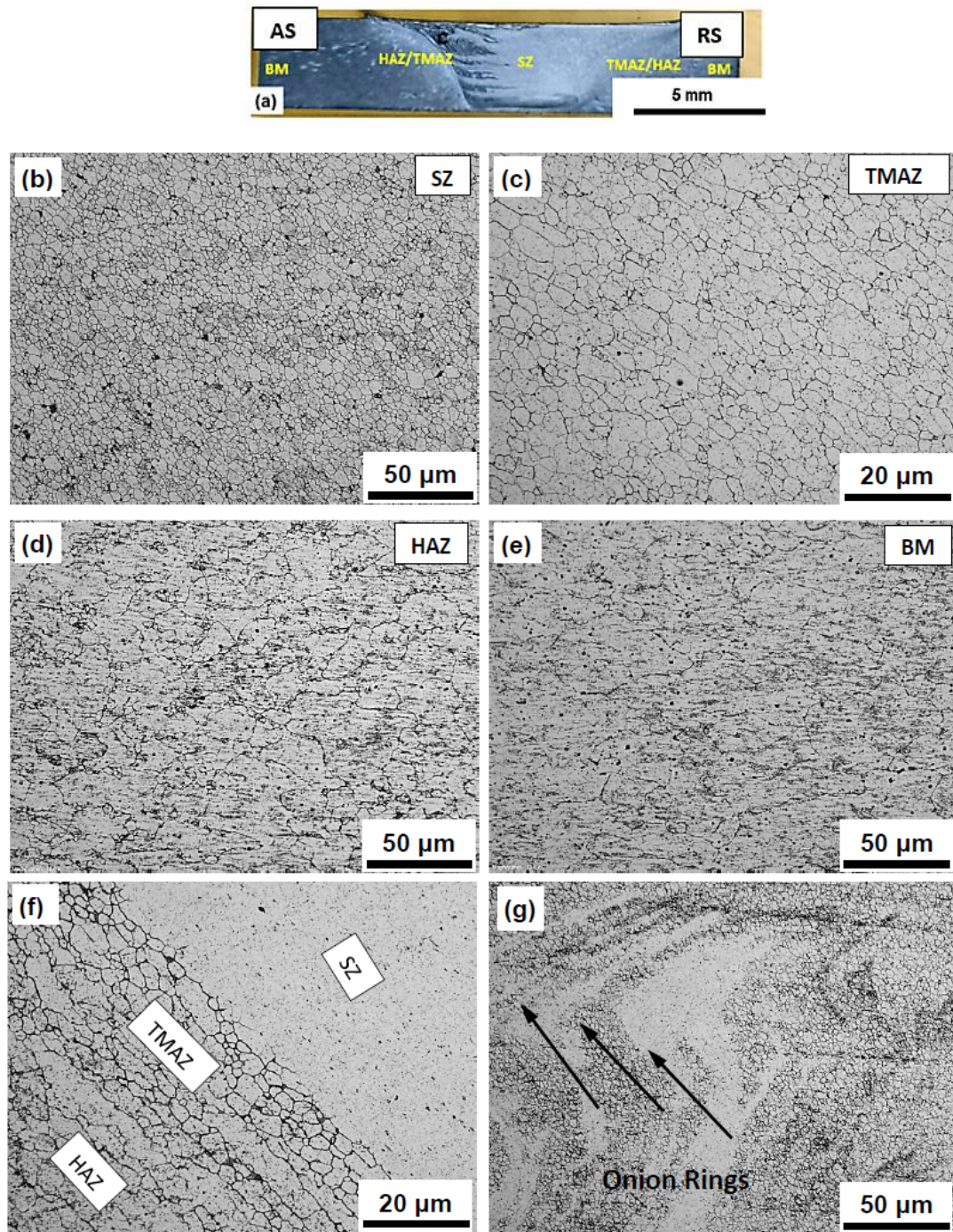


Figure 4

(a) Overview of the FSWed AA6061 obtained at a tool rotational rate of 1400 rpm and a welding speed of 1 mm/s with (b) to (g) showing the microstructures in the different weld regions as indicated in (a).

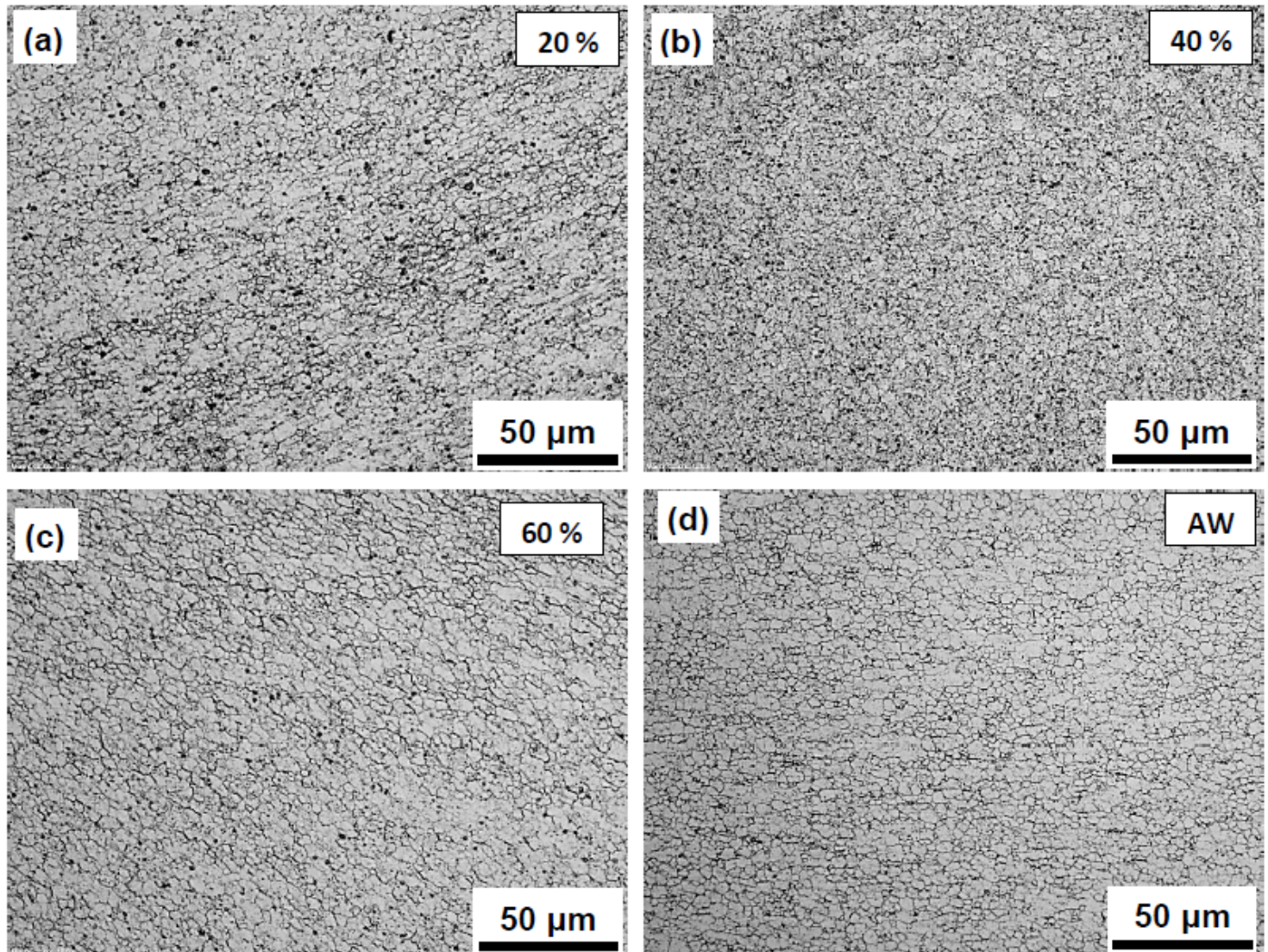


Figure 5

Optical microstructure images of SZ for different Cu Donor material thicknesses 20% (a), 40% (b), 60% (c), and As-welded condition (d).

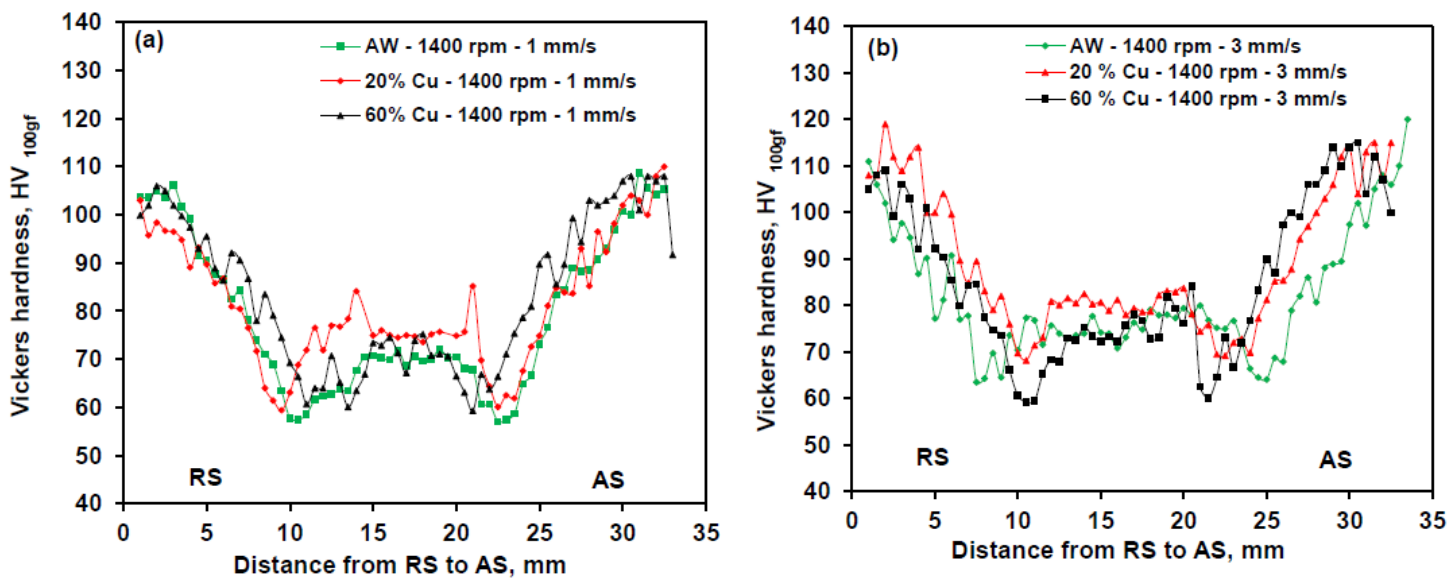


Figure 6

Micro-hardness profiles of a FSW with and without donor material (a) 1400 rpm, 1mm/s, (b) 1400 rpm, 3 mm/s.

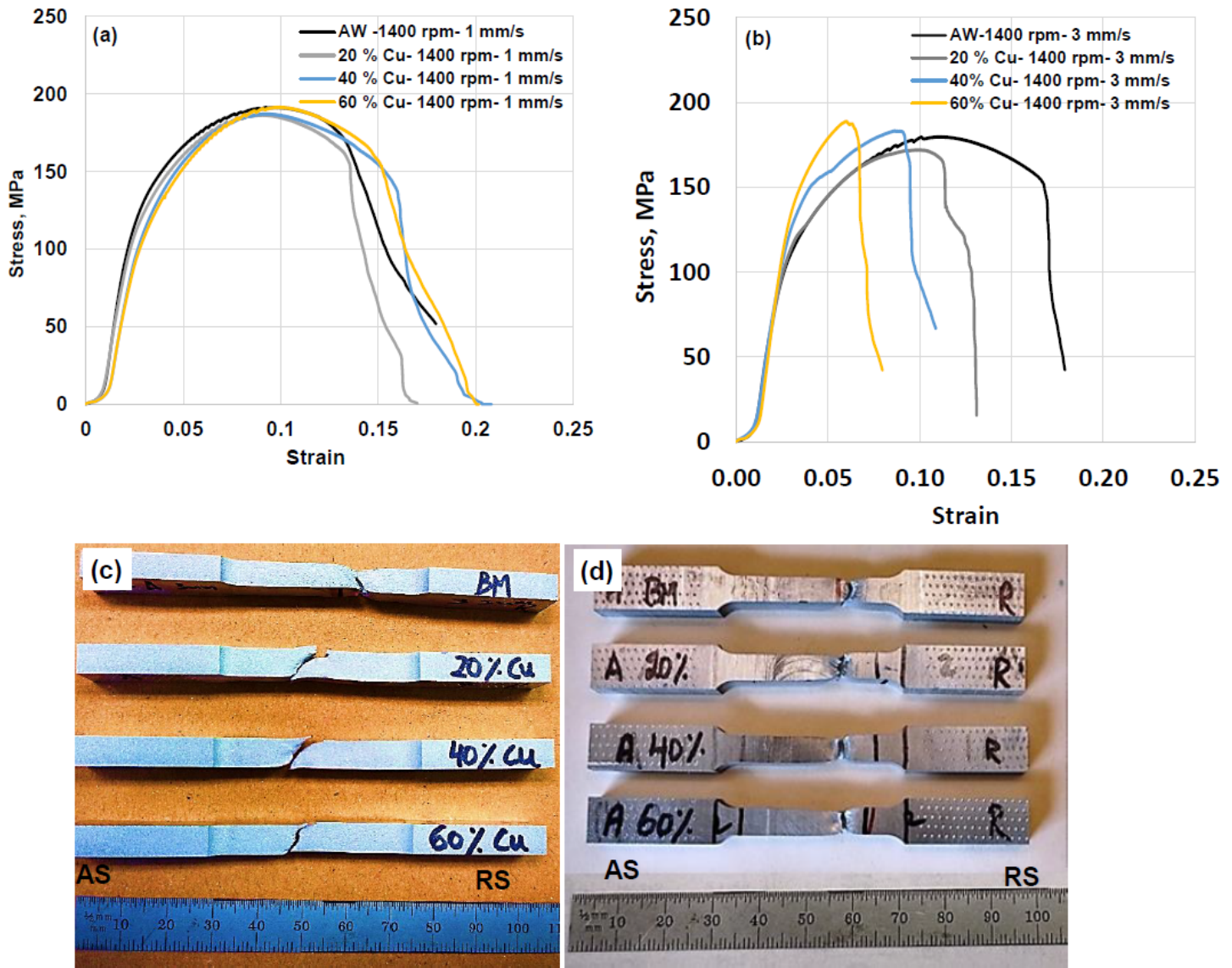


Figure 7

Tensile test plots of with and without donor material: 1400 rpm, 1 mm/s (a), and 1400 rpm, 3 mm/s (b), Tensile tested fractured samples of 1400 rpm, 3mm /s (c), and Fractured samples of 1400 rpm, 1 mm/s (d).

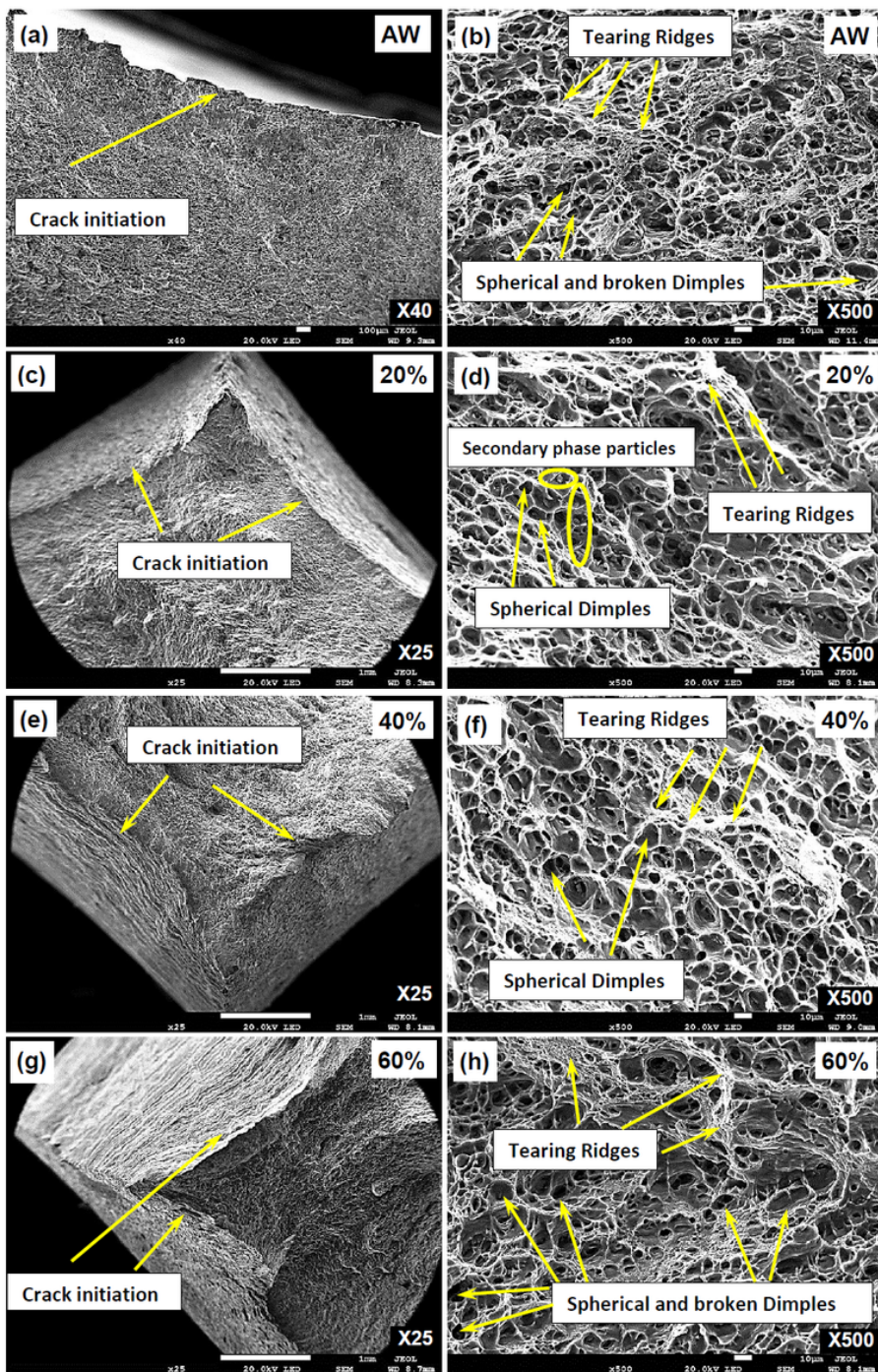


Figure 8

SEM Fractography images for 1400 rpm and 1 mm/s welding condition after tensile test, AW samples shows spherical and broken dimples (a-b), 20 % Cu donor specimen shows some secondary phase particles and dimples (c-d), 40% Cu donor specimen shows spherical dimples (e-f), and 60% Cu donor specimen shows spherical and broken dimples (g-h).

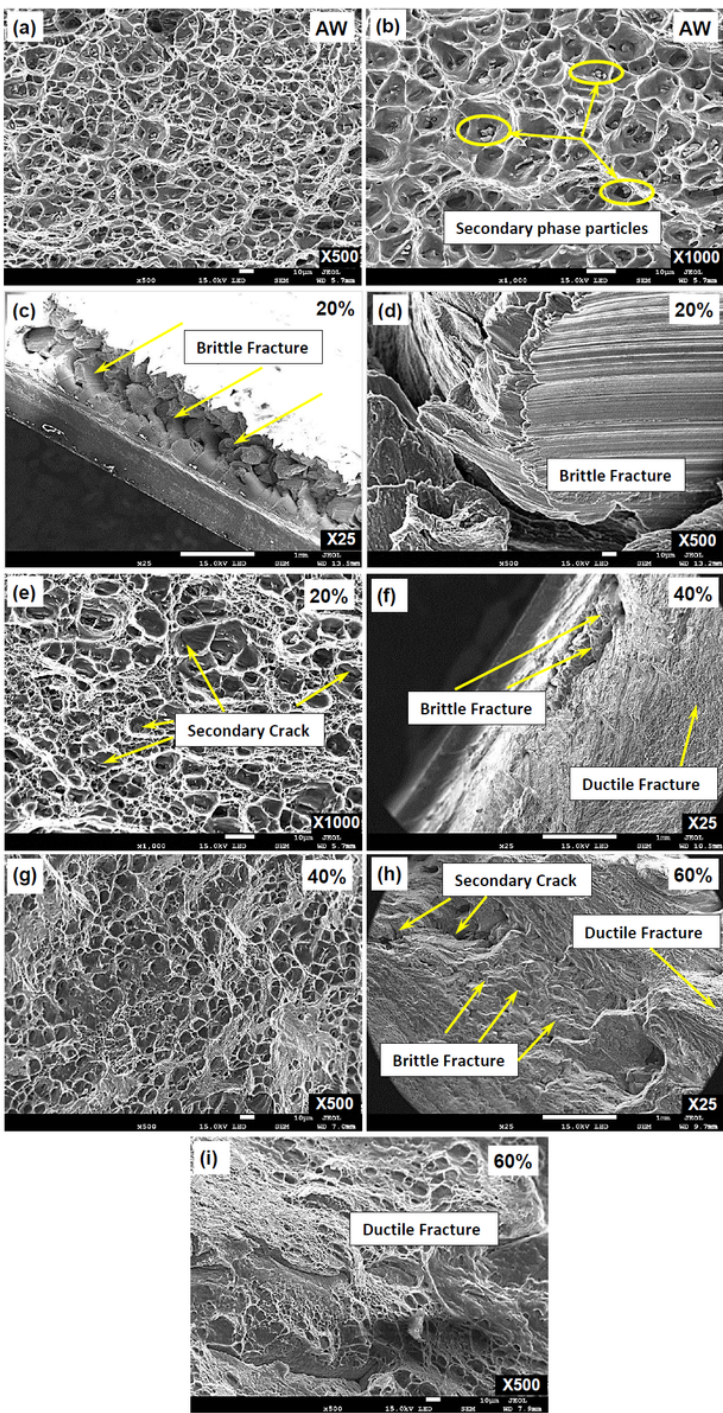


Figure 9

FE-SEM Fractography images for 1400 rpm and 3 mm/s welding condition after tensile test, AW samples show secondary phase particles (a-b), 20 % Cu donor specimen shows brittle fracture, secondary cracks(c-e), 40% Cu donor specimen shows brittle and ductile fracture images (f-g), and 60% Cu donor specimen shows secondary cracks with a combination of brittle and ductile fracture with small and elongated dimples (h-i).